The under-explored possibilities of ground state carbonyl photochemistry

Keiran N. Rowell,[†] Scott H. Kable,[†] and Meredith J. T. Jordan*[,‡]

[†]*School of Chemistry, University of New South Wales, Sydney*
[‡]*School of Chemistry, University of Sydney, Sydney*

E-mail: meredith.jordan@sydney.edu.au
Phone: +61 2 9351 4420 . Fax: +61 2 9351 3329

Abstract

Carbonyls are among the most abundant volatile organic compounds in the atmosphere, and their C=O chromophores allow them to photolyse. However, carbonyl photolysis reactions are not restricted to the excited state: the C=O chromophore allows relaxation to, and reaction on, the ground state, following photon absorption.

In this paper, the energetic thresholds for eight ground state reactions across twenty representative carbonyl species are calculated using double-hybrid density functional theory. Most reactions are found to be energetically accessible within the maximum photon energy available in the troposphere, but are absent in contemporary atmospheric chemistry models.

Structure–activity relationships are then elucidated so that the significance of each reaction pathway for particular carbonyl species can be predicted based upon their class. The calculations here demonstrate that ground state photolysis pathways are ubiquitous in carbonyls and should not be ignored in the analysis of carbonyl photochemistry.

Introduction

The importance of the ground state in carbonyl photochemistry

Physical chemistry research in past couple of decades has lead to the discovery of ground state photolysis channels in carbonyls driven by photon absorption: from more unorthodox reaction pathways like the class of 'roaming' reactions,[1–5] to conventional S_0 transition state (TS) reactions.[6–9] Despite the growing evidence for the significance of ground state photochemistry across a range of carbonyls, at photolysis energies accessible from the absorption of actinic tropospheric photons ($\lambda > 300$ nm), this ground state photochemistry is almost entirely absent from the reaction schemes of contemporary atmospheric models.[10–13]

Actinic UV photon absorption electronically excites the carbonyl C=O chromophore, and so tropospheric carbonyl reactions are commonly associated with the excited state. However, the orbital structure of the C=O chromophore provides a relaxation route to the electronic ground state on a timescale competitive with reactive dissociation.

While selection rules dictate that photon absorption will excite the carbonyl to the first excited singlet state (S_1), reaction on S_1 requires high energies and so the S_1 state is typically bound in tropospheric contexts.[14] Intersystem crossing (ISC) from S_1 to the excited triplet

state (T_1) should be formally spin-forbidden, however carbonyl S_1 and T_1 minimum energy geometries are almost identical and the energetic separation between them is small, allowing fast $S_1 \rightarrow T_1$ ISC rates.

The T_1 state minimum energy geometry is both energetically separated and geometrically dissimilar from the ground state (S_0) minimum — the RCO group is distorted to be pyramidalised on the S_1 and T_1 states, but is planar on S_0.[15] However, the non-bonding ground-state n orbital of the C=O chromophore is approximately orthogonal to antibonding π^* excited state orbital. This means the change in electron spin angular momentum in a carbonyl $T_1 \rightarrow S_0$ relaxation is accompanied by an orbital angular momentum change as the electron transitions between the π^* and n orbitals, resulting in overall conservation of angular momentum.[16] This results in relatively high $T_1 \rightarrow S_0$ ISC rates as dictated by El-Sayed's rule.[17] As a consequence, reaction on S_0 can be of far greater importance to carbonyl photochemistry than might be naïvely expected.

Carbonyl relaxation to S_0 is non-radiative,[18,19] and so a vibrationally 'hot' ground state molecule is generated that retains the absorbed UV photon energy (up to ∼400 kJ/mol in the troposphere). These photoexcited S_0 carbonyls are conformationally flexible and have far higher internal energies than is typically accessed in thermal distributions in the troposphere (∼15°C at sea level, down to −55°C at the tropopause).[20] This makes the number of possible photodissociation and photoisomerisation pathways to consider for each carbonyl quite large, particularly in consideration of the vast diversity carbonyl species in the atmosphere.[21]

Furthermore, the molecular structure of certain classes of carbonyls cause them to have mostly inaccessible excited state photolysis thresholds, and in these species photochemistry on S_0 will be not only important, but dominant.

Quantum chemistry calculations on carbonyls that have an α,β-unsaturated double bond predict that excited state α-bond cleavage reactions are inaccessible at tropospheric energies for these species,[14] and ground state photoisomerisation will be their dominant photochemical fate in the atmosphere.[6] This is supported by FT-IR experiments at actinic wavelengths on these α,β-unsaturated carbonyls (specifically, acrolein and methacrolein) where ground state photoproducts are the major contributors to quantum yields (QYs).[22] Photolysis on S_0 is therefore significant for carbonyls where excited state reactions are inhibited, and these pathways have received little attention in atmospheric modelling. Atmospheric models would benefit from the inclusion of S_0 reactions in their photolysis schemes to remedy discrepancies between modelling and field observations in cases where S_0 photolysis is important.

The omission of ground state photochemistry could have significant implications: carbonyls are ubiquitous volatile organic compounds (VOCs) in the troposphere[23,24] with high relative abundance (in the pptV–ppbV range),[25] so carbonyl reactions with QYs of only a few percent could cumulatively have a large impact on tropospheric chemistry if the reactions are accessible across many carbonyl classes.

To make sense of the expanded reaction possibilities presented by photochemistry on the ground state, we wish here to derive structure-activity relationships (SARs) for S_0 carbonyl photolysis that allow an *a priori* estimate, from a molecular structure alone, of how important it is to include particular ground state photolysis reactions in the atmospheric modelling of carbonyl species.

The known ground state photochemistry of acetaldehyde

One of the simplest aldehydes, acetaldehyde (CH_3CHO), serves as an example for the diversity of observed ground state pathways in carbonyls. Known photolysis pathways for acetaldehyde are listed in Scheme 1 below.

Reactions 1 and 2 correspond to Norrish Type I homolytic cleavage of either carbonyl α-bond. The excited state versions of these reactions account for the majority of photolysis QYs in small carbonyls.[26,27] Reaction 1 forms the larger alkyl radical, which is generally more stable due to hyperconjugation, while reaction 2 forms the smaller alkyl radical. Reactions 1 and 2

$$
\begin{aligned}
&CH_3CHO + h\nu \\
&\longrightarrow CH_3^{\bullet} + HCO^{\bullet} && (1)\\
&\longrightarrow CH_3CO^{\bullet} + H^{\bullet} && (2)\\
&\longrightarrow CH_4 + CO\ (\textit{decarbonylation}) && (3)\\
&\longrightarrow CH_4 + CO\ (\textit{roaming}) && (4)\\
&\longrightarrow H_2C{=}CH(OH) && (5)\\
&\longrightarrow H_2 + H_2C{=}C{=}O && (6)
\end{aligned}
$$

Scheme 1: Experimentally observed photolysis pathways in acetaldehyde.

have been designated the NTI*a* and NTI*b* reactions, respectively, in previous work by the authors[14] where the photolysis thresholds for reactions 1 and 2 were calculated on S_1, T_1. The NTI reactions are barrierless on S_0 and so are characterised by their asymptotic dissociation energies.[14,28]

It should be noted that, at high energies (482 kJ/mol / 248 nm), the generation of the hydrogen radical in reaction 2 has been argued to arise from a step-wise process triple fragmentation process ($CH_3CO \longrightarrow HCO^{\bullet} + CH_3^{\bullet} \longrightarrow H^{\bullet} + CO + CH_3^{\bullet}$),[29] rather than direct dissociation to $CH_3CO^{\bullet} + H^{\bullet}$.[30]

Reactions 3 and 4 generate the same photolysis products, $CH_4 + CO$, but *via* different mechanisms and consequently have distinct internal energy distributions. Reaction 3 occurs *via* a canonical TS decarbonylation pathway,[31,32] while reaction 4 occurs *via* a 'roaming' pathway where partly dissociated fragments become trapped in each other's attractive van der Waals well and ultimately recombine to generate closed-shell molecular products.[33] In fact, roaming is the dominant pathway to forming $CH_4 + CO$ in acetaldehyde photolysis,[34] and should not be neglected when considering S_0 photolysis products.

The mechanism of roaming reactions are inherently tied to their dynamics and do not follow a minimum energy pathway over a TS,[2] and so roaming reactions are not able to be characterised with the potential energy surface calculations of the type contained in this current paper. It is therefore unlikely that SARs for roaming reactions could be developed from calculated molecular structures and threshold energies alone. The roaming mechanism is, however, intimately linked with barrierless S_0 NTI dissociation.[35–38] More sophisticated methods to understand the roaming process can be found in other work.[35,36,39]

Reaction 5 does not involve dissociation, but instead the molecule phototautomerises to an enol through an intramolecular hydrogen transfer to the C=O oxygen. It was only in the past decade that a rigorous prediction of this keto-enol phototautomerisation mechanism was provided,[8] and was subsequently followed by direct observation of the reaction in Fourier-transform infrared (FT-IR) spectroscopy experiments.[40] Recently, keto-enol phototautomerisation was shown to be an important route to formation of atmospheric formic acid from acetaldehyde, that was missing from atmospheric models.[41] While phototautomerisation to other isomers of acetaldehyde (oxirane, methylhydroxycarbene) are hypothetically available at tropospheric photon energies, the barriers to reversal are small for these isomers and so are unlikely to be collisionally stabilised before reversion to the parent carbonyl occurs.[42] Furthermore, no experimental evidence so far has clearly indicated the participation of any of these other isomers in tropospheric photolysis, and so these isomers are excluded from further consideration within this paper.

Finally, reaction 6 is photodissociation to H_2 and a ketene (ethenone). Despite this ketene dissociation pathway having one of the lowest reaction barriers according to quantum chemical calculations, direct observation of this reaction was only reported in 2019.[43] This demonstrates that the QYs of these S_0 reactions depend not only on energetic thresholds, but also on kinetic factors. Interestingly, the observed product state distributions of this ketene dissociation pathway do not match those from trajectory simulations of the canonical TS pathway,[43] indicating the reaction dynamics of this mechanism needs to be investigated further.

From this one example of the acetaldehyde molecule, it can be seen that there are many

photolysis pathways available to S_0 carbonyls, beyond the standard NTI excited state α-bond cleavage reaction. Most of these reaction channels are treated inconsistently, or are entirely absent, in contemporary atmospheric chemistry models.

The Master Chemical Mechanism (MCM)[10] includes only reaction 1, the NTI*a* photolysis channel. The justification given for excluding the other photolysis pathways is that reaction 2, NTI*b* photolysis, has a QY of <0.06 across the actinic range, while the production of CO — reactions 3 & 4 — only becomes appreciable above the actinic energy range (<290 nm).[26,44,45] GEOS-Chem,[12] however, does include dissociation to CH_4 + CO as well as the NTI*a* reaction,[12,46] but does not include any mechanistic information and so can not distinguish between TS decarbonylation or roaming contributions.[34]

So, not only do contemporary atmospheric models disagree on which photolysis pathways are important for inclusion, they also lack the detailed physical chemistry insight to determine the mechanism observed photoproducts arise from. While empirical reaction rate data[47] can be used to model the atmospheric chemistry of individual species, predictive modelling for species that have not been subject to experimental studies requires mechanistic and energetic insight.

Accordingly, this paper uses quantum chemistry calculations to predict carbonyl ground state photolysis thresholds on a dataset of 20 species. This dataset includes all species that have explicit photolysis reactions in the MCM,[10,48] and encompasses a variety of representative structural features so that any trends in calculated S_0 photolysis energies can be extended to predictive SARs for other carbonyl species.

Dataset of S_0 reactions investigated

The 20 carbonyl species studied in this work are shown in Scheme 2, and highlight the diversity of carbonyl classes surveyed. They are the same set of molecules for which excited state NTI photolysis thresholds have already been calculated.[14] Reaction threshold energies throughout this paper will be colour-coded according to the carbonyl classes labelled in Scheme 2.

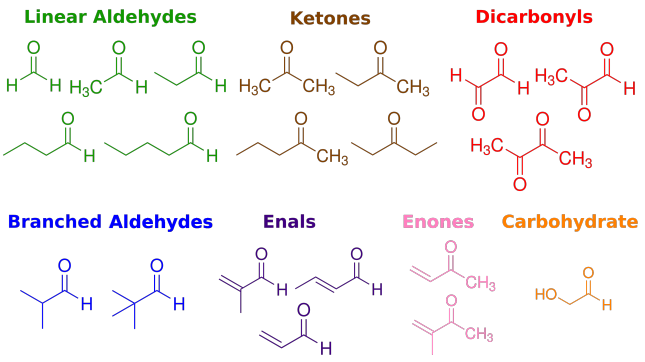

Scheme 2: The 20 carbonyl species studied here, organised and colour-coded according to carbonyl class.

Eight types of ground state reactions are calculated for the carbonyls above:

- Decarbonylation (CO–loss).
- Concerted triple fragmentation (TF).
- Norrish Type III β-H transfer (NTIII).
- H_2–loss from hydrogens at the formyl and α positions (formyl+α).
- H_2–loss from hydrogens at the α and β positions (α+β).
- H_2–loss from hydrogens at the β and γ positions (β+γ).
- Keto–enol tautomerisation.
- Enal–ketene tautomerisation.

The list above summarises the reactions relevant to tropospheric photolysis energies. It is not exhaustive of all hypothetical carbonyl ground state reactions, and excludes: several isomerisation pathways and some S_0 dissociation pathways that are above the actinic photon energies, step-wise triple fragmentation reactions, 'roaming' reactions, and barrierless S_0 homolytic bond cleavages.

Many of these additional S_0 pathways have been calculated for butanal in the PhD work of Shaw,[49] and only the S_0 reactions that were predicted to be energetically and conformationally favourable for butanal actinic photon energies

are studied here for other carbonyl species. Several additional potential isomerisation pathways are also not considered in this paper, as they are reversible and are generally seen experimentally to be minor pathways,[50] since the parent carbonyl is the most thermodynamically stable isomer in all cases here.

Hypothetically, homolytic bond cleavage can occur across any bond of a 'hot' S_0 molecule with high internal energy. 19 such homolytic cleavage reactions in butanal have been calculated in the work of Shaw.[49] In butanal, the S_0 asymptotic energy of cleaving the α,β-bond to form $CH_3CH_2^{\bullet}$ + $^{\bullet}CH_2CHO$ was predicted by M06-2X quantum chemistry calculations to be 336 kJ/mol, which was lower than the S_0 NTI*a* asymptotic energy of 341 kJ/mol. However, only the S_0 NTI*a* reaction was found to be important in predicting QYs from master equation simulations.[49] Therefore, only the asymptotic energies for S_0 NTI*a* dissociation are important for carbonyl photochemistry, and they have been calculated in earlier work.[14]

Butanal also provides a good illustration of possible ground state photochemistry since all the S_0 reactions listed above, bar a phototautomerisation that converts enals to ketenes, are hypothetically available in the photolysis of butanal. Calculated threshold energies of these S_0 reactions are shown in Figure 1 below to give an example of the relative energetics of these pathways. In the following figures, a solid purple line at 400 kJ/mol is used to indicate the approximate upper limit of photon energy available in the troposphere.

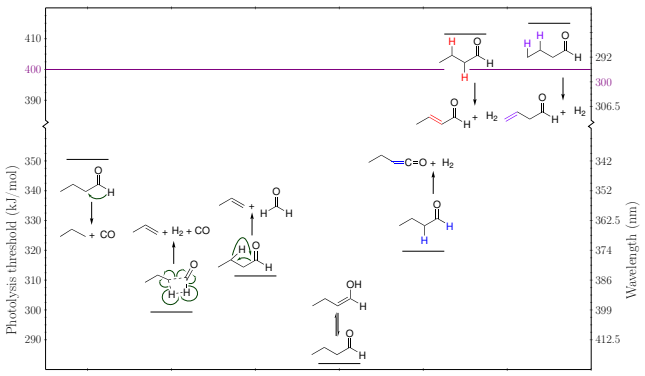

Figure 1: Calculated S_0 reaction threshold energies in butanal. Seven of the eight S_0 reaction types studied in this paper are illustrated.

The quantum chemical method to calculate these reaction energies, B2GP-PLYP/def2-TZVP, has been found to give errors of less than 8 kJ/mol across the entire range of benchmark data,[51] and has been validated against experimental data for carbonyls specifically in an earlier publication.[14] This B2GP-PLYP/def2-TZVP method is used for all energies reported herein. Details of the theoretical methods used to perform the quantum chemical calculations reported here are provided at the end of the paper.

Results

Calculated S_0 photolysis thresholds

Calculated photolysis thresholds for the eight S_0 reaction types across the 20 species considered here are reported in Table 1. Note that TF refers to concerted, rather than step-wise, triple fragmentation reactions. For glycolaldehyde, several reactions involve the OH hydrogen atom, including TF and the two possible H_2–loss mechanisms.

With the exception of some H_2–loss reaction types, and a few NTIII thresholds, all the S_0 thresholds are calculated to be below the 400 kJ/mol upper limit for solar radiation in the troposphere. Note that the intensity of the solar radiation increases with decreasing photon energy below 400 kJ/mol, while the absorption spectra of saturated carbonyls extends to photon energies of ~360 kJ/mol (λ ~330 nm), and to even lower energies for unsaturated species.[52] This means almost all of the calculated ground state photolysis reactions in Table 1 theoretically available to photoexcited atmospheric carbonyls, provided they can cross to S_0 before excited state reaction occurs.

Each ground state photolysis pathway in Table 1 will be discussed in separate sections below. Chemically rationalised SARs will be drawn from the calculated photolysis thresholds energies, and comparison made to theoretical and experimental data where available. The three H_2–loss channels will be discussed together in one section.

Table 1: Ground state photolysis thresholds for all molecules considered here. All values are zero-point corrected and calculated at the B2GP-PLYP/def2-TZVP level of theory. (kJ/mol)

				H_2–loss (*H positions)*			Tautomerisation	
	CO–loss	TF[a]	NTIII	(*formyl*+α)	(α+β)	(β+γ)	Keto–enol[b]	Enal–ketene
Aldehydes								
Formaldehyde	352	—	—	—	—	—	—	—
Acetaldehyde	352	—	—	337	—	—	281	—
Propanal	348	295	332	314	427	—	278	—
Butanal	351	299	311	320	410	516	282	—
Pentanal	350	294	310	317	409	499	281	—
2-Methylpropanal	345	304	330	310	421	—	296	—
Pivaldehyde	342	306	323	—	—	—	—	—
Ketones:								
Acetone	—	—	—	—	—	—	275	—
Butanone	—	—	354	—	447	—	274	—
Pentan-2-one	—	—	316	—	416	513	270	—
Pentan-3-one	—	—	350	—	442	—	276	—
α,β-Unsaturated:								
Acrolein	360	343	394	373	—	—	291	297
Crotonaldehyde	375	351	387	386	—	—	294	299
Methacrolein	362	338	379	—	—	—	—	291
MVK	—	—	417	—	—	—	270	—
MIPK	—	—	395	—	—	—	—	—
Dicarbonyls:								
Glyoxal	321	247[c]	—	—	—	—	—	—
Methylglyoxal	333	330	400	—	—	—	—	—
Diacetyl	—	—	415	—	—	—	—	—
Carbohydrates:								
Glycolaldehyde[d]	345	229[e]	—	292	384[f]	—	272	—

[a] Concerted triple fragmentation reactions. Step-wise triple fragmentations (*e.g.* $H_2CO \longrightarrow HCO^{\bullet} + H^{\bullet}$; $HCO^{\bullet} \longrightarrow H^{\bullet} + CO$) are not included here.

[b] Lowest energy enol isomer reported here. See Section S5 of the supporting information for more details.

[c] This concerted triple fragmentation transition state for glyoxal differs qualitatively from other species. In glyoxal it involves a 4-centred transition state involving two formyl-Hs, whereas in other carbonyls a formyl-H and a β-H is involved.

[d] Several reactions listed here are not directly analogous to those in other carbonyls, as the transition state involves the hydrogen from the OH moiety.

[e] The β-H for the triple fragmentation transition state in glycolaldehyde comes from the OH moiety.

[f] The β-H for this H_2–loss transition state in glycolaldehyde combines with the OH hydrogen.

Discussion

Decarbonylation (CO–loss)

Decarbonylation reactions involve CO–loss from the parent molecule. In aldehydes, the decarbonylation reaction is a transfer of the formyl hydrogen to the main alkyl chain, forming CO and an alkane: $R{-}(C{=}O){-}H \longrightarrow CO + RH$. Decarbonylation has been established in photolysis experiments on specific aldehydes as an S_0 process.[27,53,54] Decarbonylation is uncommon in solvent-phase ketones, requiring catalysts or special reaction conditions,[55] since transfer of an alkyl group involves greater steric strain, and activation of C−C bonds is more difficult than for C−H bonds. The gas-phase photolytic formation of CO and a hydrocarbon *via* a single-step decarbonylation reaction has not been observed in ketones, but is commonly observed in aldehydes.[27,54,56] As such, decarbonylation pathways are only calculated here for the aldehydes, and the thresholds energies are shown in Figure 2.

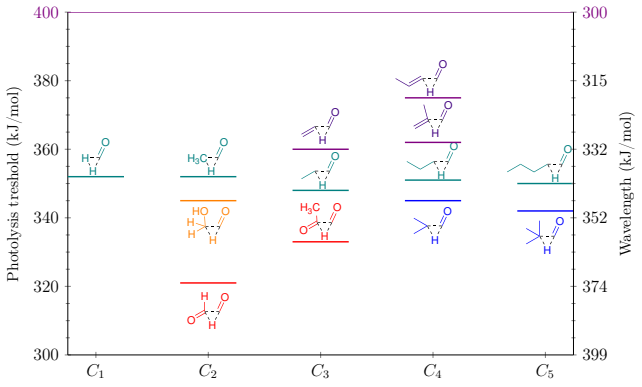

Figure 2: Decabonylation S_0 photolysis thresholds, computed at the B2GP-PLYP/def2-TZVP level of theory.

One trend apparent in Figure 2 is that extension of the main alkyl chain has little effect on the decarbonylation threshold, with formaldehyde through to pentanal all predicted to have ∼350 kJ/mol thresholds. The predicted decrease in threshold upon branching at the α-position is ∼5 kJ/mol; far less than was predicted for NTI reactions on S_1, T_1, and S_0 using the same level of theory.[14] This small decrease is reflected in the decarbonylation thresholds predicted for 2-methylpropanal (345 kJ/mol) and pivaldehyde (342 kJ/mol), and is at the ±4 kJ/mol 'chemical accuracy' limit of the quantum chemical calculations.[57]

The α,β-unsaturated enals are predicted to have higher decarbonylation thresholds than the saturated aldehydes, as this process involves breaking the delocalised α-bond from the main alkyl chain to the carbonyl moiety. For acrolein and methacrolein this increase is predicted to be on the order of 10 kJ/mol. Further delocalisation of the π system is predicted to increase the threshold higher still, at 375 kJ/mol for crotonaldehyde.

The dicarbonyls are predicted to have the lowest decarbonylation thresholds. This is consistent with the two electron-withdrawing oxygen substituents reducing the electron density between the carbonyl moieties, weakening the α-bond. The 321 kJ/mol threshold in glyoxal is increased to 333 kJ/mol in methylglyoxal. This increase likely originates from an increase in the central C−C bond strength with addition of the CH_3 group, and possibly some small degree of steric penalty. Geometrically labelled TS structures for these reactions are displayed in Figure S1 in the supporting information.

All decarbonylation thresholds for the aldehydes, saturated or otherwise, are predicted to be accessible at the maximum tropospheric photon energy of 400 kJ/mol. However, decarbonylation QYs are low for large carbonyls, measured to be ∼0.01 for butanal[54] and not detected in propanal[50] — though in small carbonyls the decarbonylation QYs are higher, ∼0.02 in acetaldehyde[58] (where the majority of CO is from 'roaming'),[34] and ∼0.5 in formaldehyde[59] (a molecule with a high NTI*a* photolysis threshold).

While the α-dicarbonyls glyoxal and methylglyoxal and predicted to have the lowest decarbonylation thresholds within the "small" carbonyl dataset, they also had the lowest NTI photolysis thresholds,[14] resulting in competition between NTI dissociation and decarbonylation in the actinic energy range.[45,60] Indeed, photolysis of methylglyoxal is dominated by the NTI reaction in the actinic energy range.[45,61] For glyoxal, following photolysis, FT-IR experiments cannot directly determine the mechanism of production of CO as it can arise from both primary decarbonylation and the TF reaction: H(C=O)−(C=O)H ⟶ H_2 + 2 CO, as well as from secondary radical-radical reactions arising from NTI, *e.g.* $HCO^{\bullet} + HCO^{\bullet} \longrightarrow H_2CO + CO$. In the actinic energy range, however, it is known that the photoproducts of glyoxal are dominated by either NTI or decarbonylation reactions, with TF significant only at higher energy.[45,62]

Triple fragmentation (TF)

For the purposes of this paper, the TF reaction is defined as a concerted S_0 reaction where all three photoproducts are formed simultaneously *via* a single TS. More specifically, this section focuses on TF reactions that form H_2. Thus, for saturated aldehydes, the TF reaction considered is: RH−CH_2−(C=O)H ⟶ R=CH_2 + H_2 + CO.

For the enals, the hydrocarbon product will be an alkyne. For the dicarbonyls, TF will form H_2, CO, and another carbonyl. Glycolaldehyde is an atypical carbonyl, and so the TF reac-

tion for glycolaldehyde has been calculated in this work to be H_2 formation *via* combination of the formyl hydrogen and the OH hydrogen. This alternative TF pathway has not been previously proposed in the photolysis of glycolaldehyde.[45,63–66]

Predicted S_0 TF thresholds are shown in Figure 3 below. In all cases but one, TF involves a sterically favourable 5-centre concerted TS involving H-loss from a β-hydrogen. Glyoxal is the exception, where TF occurs *via* a 4-centre TS involving the two formyl hydrogens.

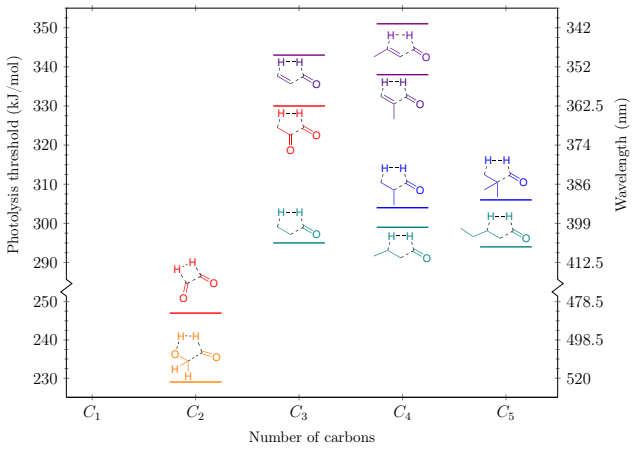

Figure 3: Concerted S_0 triple fragmentation photolysis thresholds, computed at the B2GP-PLYP/def2-TZVP level of theory.

The S_0 TF photolysis thresholds for the saturated aldehydes are not predicted to be significantly affected by chain extension, with thresholds of: 295, 299, and 294 kJ/mol for propanal, butanal, and pentanal, respectively.

The predicted effect of alkyl branching at the α-position is inconsistent and small. Branching at the α-position is predicted to raise the thresholds to 304 kJ/mol for 2-methylpropanal and 306 kJ/mol for pivaldehyde, but is predicted to lower the threshold for methacrolein (338 kJ/mol) compared to acrolein (343 kJ/mol).

A more clear-cut SAR for TF can be derived from the bond order near the site of bond cleavage, rather that the degree of substitution. The TF thresholds of enals are predicted to be significantly higher than for saturated aldehydes, at 343, 338, and 351 kJ/mol for acrolein, methacrolein, and crotonaldehyde, respectively. This reaction threshold bond increase of ∼40 kJ/mol compared to saturated species is beyond the ∼10 kJ/mol increase seen in the decarbonylation reaction for breaking a delocalised C=C bond on the S_0 state. In the α,β unsaturated species, the 5-centre TF TS is strained, with the ∠C−C−C backbone angles deviating significantly from their equilibrium values. The resulting steric penalty, which is increased relative to saturated species because of bond delocalisation, leads to increased TF thresholds for these α,β-unsaturated species. The structures of these TF TSs are displayed in Figure S2 in the supporting information.

The predicted S_0 TF photolysis thresholds of the two α-dicarbonyls, glyoxal and methylglyoxal, differ markedly by 83 kJ/mol. This is because their TF TS structures, and reaction products, are qualitatively different. Methylglyoxal has a 5-centre TS that involves strain across the O=C−C=O "backbone" and also forms a relatively high energy ketene photoproduct. Glyoxal has a 4-centre TF TS with less overall strain and yields H_2 and two CO molecules, resulting in an atypically low S_0 TF threshold.

The lowest TF threshold of all the carbonyls in the dataset, 229 kJ/mol, was calculated for glycolaldehyde, which has a qualitatively different TS in that the H_2–loss channel arises from combination of the formyl-hydrogen and the OH-hydrogen, rather than involving a hydrogen on the alkyl backbone. The OH-hydrogen is more labile than a hydrogen in a C−H bond, and the ∠C−OH moiety angle involves minimal ring strain (see Figure S2k in the supporting information).

Norrish Type III β−H transfer (NTIII)

Alongside the Norrish Type I and II reactions, the lesser known 'Norrish Type III' (NTIII) reaction was proposed in 1965 by Zahra and Noyes to explain the observation of acetaldehyde and propene as photoproducts of 3-methylbutan-2-one.[67] The NTIII reaction involves a 4-centre TS, with β-hydrogen transfer from the backbone to the carbonyl moiety leading to formation of an aldehyde and an alkene:

$R{-}CH_2{-}CH_2{-}(C{=}O)R' \longrightarrow R{-}CH{=}CH_2 + H(C{=}O)R'$.

This NTIII reaction was found to be a minor channel, and has received less attention than excited state Norrish reactions, or the S_0 TF and decarbonylation reactions. However, since the alkene photoproduct from NTIII can be the same molecule as from other S_0 reactions (TF, H_2-loss), the photolysis thresholds of the NTIII need to be well understood to disambiguate any uncertainty when interpreting which mechanism a photoproduct arises from in an photolysis experiment. Moreover, the aldehyde formed through the NTIII reaction is photoactive and so could undergo further photolysis reactions, again complicating the interpretation of photolysis experiments.

Shaw was able to conclude, through wavelength-dependent data and computational modelling, that observed NTIII photoproducts likely arise from a concerted S_0 reaction and are not the result of excited state or radical disproportionation reactions.[49] Following on from this evidence that NTIII is a distinct and significant reaction mechanism, in Figure 4 we show the NTIII thresholds for the carbonyls calculated here.

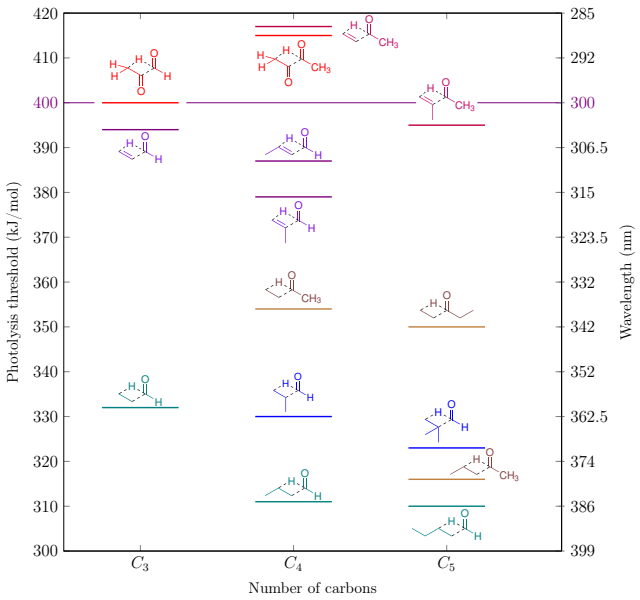

Figure 4: Norrish Type III S_0 photolysis thresholds, computed at the B2GP-PLYP/def2-TZVP level of theory.

The calculated S_0 NTIII thresholds shown in Figure 4 vary across a large energy range, from 310–417 kJ/mol, in contrast to the other S_0 reactions examined in this paper. In certain unsaturated species (glyoxal, methylglyoxal, and methyl vinyl ketone) the calculated NTIII thresholds are at or above the 400 kJ/mol upper range of the actinic energies. The NTIII thresholds of the other α,β-unsaturated carbonyls lie in the ∼380–400 kJ/mol range. These predictions of S_0 NTIII barriers above or only slightly below available tropospheric photon energies indicate that, for the majority of the α,β-unsaturated carbonyls in the troposphere, S_0 NTIII reactions will not occur even if the S_0 state were populated.

Focussing on the saturated species in Figure 4, their NTIII thresholds lie in a broad energy range from ∼310–355 kJ/mol. One discernible trend is that NTIII thresholds decrease when the main alkyl chain is lengthened past the β-position. This is shown by a 38 kJ/mol lowering of the NTIII threshold going from butanone to pentan-2-one, and a 21 kJ/mol lowering going from propanal to butanal. The effect appears to be smaller in α,β-unsaturated carbonyls, with a 7 kJ/mol decrease in the NTIII threshold from acrolein to crotonaldehyde.

The NTIII threshold from butanal to pentanal, however, is virtually unchanged (from 311 to 310 kJ/mol), suggesting further chain lengthening past the γ-position will not result in any change to the reaction threshold. This is supported by the 4 kJ/mol difference in predicted NTIII barrier heights of butanone and pentan-3-one, which is again at the 'chemical accuracy' limit of quantum chemical calculations. Indeed, it is likely that the experimental NTIII thresholds for butanone and pentan-3-one are similar, as the second ketone alkyl substituent on the other side of the molecule does not interact with the reactive β-H transfer region. Thus a simple SAR for the NTIII reaction is that alkyl chains more than one carbon removed from the reactive β-position will not alter the NTIII photolysis threshold energy.

Branching at the α-position is predicted to decrease NTIII thresholds, though to a lesser degree than addition of a γ-carbon. The decreases are: 2 kJ/mol from propanal to 2-methylpropanal, 7 kJ/mol from 2-

methylpropanal to pivaldehyde, 15 kJ/mol from acrolein to methacrolein, and 23 kJ/mol from methyl vinyl ketone to methyl isopropenyl ketone. These decreases to NTIII thresholds upon α-branching are large enough (except between propanal and 2-methylpropanal) that they should be outside any inherent error of the B2GP-PLYP calculations. However, the difference in these magnitudes in TS stabilisation make it difficult to propose a species-independent quantitative SAR for how the NTIII threshold decreases with α-branching.

Concerted 4-centre H_2–loss

Another set of mechanisms for H_2 formation on S_0 by unimolecular dissociation are 4-centre TSs where adjacent hydrogen atoms form an H−H bond and dissociate as H_2, leaving behind a point of unsaturation in the parent carbonyl. These adjacent hydrogens can be the formyl hydrogen and α hydrogen, but as the main alkyl chain lengthens the possibilities for adjacent combinations increases to include the: α and β, β and γ, *etc.*, positions. There are thus several possible mechanisms for H_2–loss to consider in larger carbonyl species, which can be distinguished by co-photoproducts that differ in the location of the point of unsaturation.

The S_0 reaction thresholds for these H_2–loss channels are given in Table 1 and selected values are shown in Figure 5, where: solid lines denote H_2–loss from the formyl and α positions, dashed lines denote H_2–loss from the α and β positions, and dot-dashed lines denote H_2–loss from the β and γ positions. A particular carbonyl may appear multiple times in Figure 5 if it has multiple possible sites where loss of adjacent hydrogens can occur. The y-axis is broken into low, middle, and high energy sections in Figure 5 to indicate the energetic separation between H_2–loss mechanisms at different positions on the main alkyl chain. Thresholds for H_2–loss in acrolein and crotonaldehyde fall between the low and middle energy ranges and are not shown in Figure 5.

The H_2–loss thresholds shown in Figure 5 reinforces, for multiple carbonyl species, that only H_2–loss from the formyl and α positions is energetically accessible in the actinic range. Naturally, H_2–loss does not need to be considered for tropospheric ketones, since they lack a formyl hydrogen. This also rules out the need to include a concerted 4-centre H_2–loss mechanism for the atmospheric photolysis of carbonyls which lack an α-hydrogen, *e.g.* 2,2-dimethylbutanal and methacrolein. The possibilities for H_2–loss mechanisms in carbonyls with main alkyl chains longer than two carbons can also be greatly simplified — again, only a 4-centre TS involving the formyl and α hydrogen need be considered for photolysis in a tropospheric context.

Having simplified the consideration of H_2–loss channels, the task turns to determining what, if any, structural effects alter thresholds for H_2–loss from the formyl and α positions. The threshold for H_2–loss from the formyl-H and α-H positions lie in a small (314–319 kJ/mol) range for the linear aldehydes: propanal, butanal, and pentanal. However the threshold for the same TS in acetaldehyde is ∼20 kJ/mol higher, at 337 kJ/mol. It is here that the calculations on the thresholds of H_2–loss from other positions on

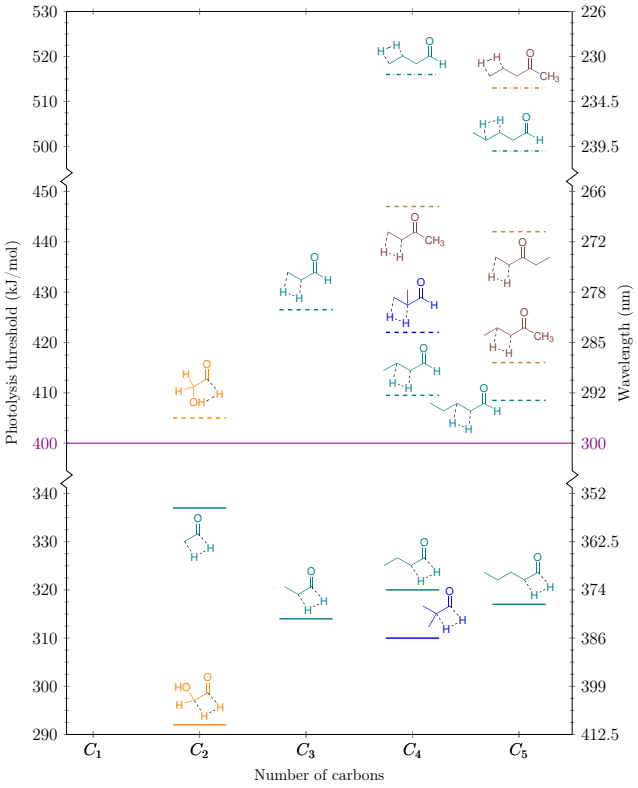

Figure 5: H_2 formation S_0 photolysis thresholds, computed at the B2GP-PLYP/def2-TZVP level of theory. Solid lines: formyl–H + α–H, dashed lines: α–H + β–H, dot-dashed lines: β–H + γ–H.

the main alkyl chain are informative in forming a SAR.

It is clear from the threshold energy separations indicated by the broken y-axis in Figure 5 that H_2–loss from the α and β position is higher than the favoured formyl and α positions. All H_2–loss thresholds from the β and γ positions are higher still. Upon examining these trends, it can be seen that the highest thresholds are predicted when H_2–loss involves removal of a hydrogen from the terminal carbon position of a molecule. The H_2–loss threshold decreases when the main alkyl chain extends past the position of hydrogen loss. This decrease is approximately 20 kJ/mol when chain extension past the site of H_2–loss first occurs, with no decrease on further chain lengthening.

For example, for H_2–loss from the formyl and α hydrogens, there is a ∼20 kJ/mol decrease in thresholds from acetaldehyde to propanal in the low energy region of Figure 5. For H_2–loss from the α and β positions a ∼20–30 kJ/mol drop occurs (*cf.* propanal and butanal, butanone and pentan-2-one, in the middle energy region). This trend is also repeated for H_2–loss from the β and γ position where a ∼20 kJ/mol drop occurs (*cf.* butanal and pentanal in the high energy region).

In contrast, minimal changes in H_2–loss thresholds are seen upon α-branching (*cf.* propanal and 2-methylpropanal in the low energy region). Similarly, no significant threshold reducing is predicted upon further extension of the main alkyl chain once the reacting hydrogens are no longer in the terminal position (*cf.* propanal and pentanal in the low energy region, butanal and pentanal in the middle energy region).

Two straightforward SARs describing the concerted 4-centre H_2–loss reactions in carbonyls can therefore be formulated. Firstly: only loss of adjacent hydrogen atoms from the formyl and α positions is important at actinic energies. Secondly: H_2–loss thresholds involving a hydrogen on a terminal carbon are ∼20 kJ/mol higher than those when the hydrogens are on non-terminal carbons.

Glycolaldehyde was calculated to have the lowest H_2–loss threshold, 292 kJ/mol, for loss of the formyl and α hydrogens. The low formyl and α H_2–loss threshold in glycolaldehyde can be rationalised in terms of the electron withdrawing nature of the OH stabilising the 4-centre TS. Despite the increased lability of hydrogen from the OH group, H_2–loss in glycolaldehyde involving the OH hydrogen to form H_2 and glyoxal was predicted to be ∼90 kJ/mol higher in energy than formyl and α hydrogen loss. Nevertheless this threshold was lower than H_2–loss from the α and β positions in the other carbonyl species.

Keto–enol tautomerisation

Many carbonyls exist in a dynamic equilibrium of two tautomeric forms: a keto form (encompassing, in this terminology, both ketones and aldehydes), and an enol form where the α-H has transferred to the carbonyl oxygen to form an OH substituent while leaving behind a point of α,β-unsaturation. This keto–enol tautomerisation is known to occur in S_0 carbonyls in aqueous solution at room temperature, though the keto tautomer is the thermodynamically favoured product.[68] This keto–enol tautomerisation has previously been speculated to explain why many carbonyls display total photodissociation and emission QYs less than unity,[67] and has recently been observed in gas-phase photolysis experiments on butanal.[8,41,69]

However, it is possible that keto–enol phototautomerisation is available in many other carbonyl species. As Shaw *et al.* note in their work modelling the formation of formic acid *via* phototautomerisation: *"Although phototautomerization of acetaldehyde does provide a source of formic acid, it alone cannot account for the factor of two or more discrepancy seen between experimental and modeled formic acid concentrations worldwide. However, the role of photo-tautomerization of other carbonyls has not been explored. For example, the known photochemistry of propanal and acetone is broadly similar to acetaldehyde, with similar tautomerization barrier heights. We might therefore expect photo-tautomerization efficiencies to be broadly similar in these carbonyls under atmospheric conditions."*[41]

The calculated keto-enol phototautomerisation thresholds calculated here and shown in Figure 6 allow comparison of whether similar

thresholds exist across all carbonyl classes.

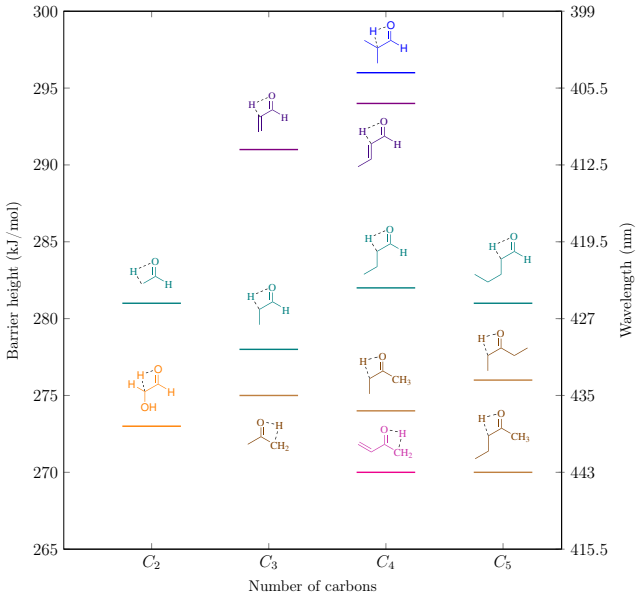

Figure 6: Keto–enol S_0 tautomerisation thresholds, computed at the B2GP-PLYP/def2-TZVP level of theory.

It is important to note that often two or more keto-enol tautomerisation pathways exist for a carbonyl. Mainly, tautomerisation to the *trans*-enol or the *cis*-enol, or in asymmetric ketones tautomerisation with hydrogens from either alkyl ketone substituent. As covered in more detail in Section S5 of the supporting information, isomerisation to the *trans*-enol is typically calculated to have a 20 kJ/mol lower threshold than isomerisation to the *cis*-enol. This is because in the *trans*-enol the bulky alkyl substituent is pointing away from the enol OH group, while in the *cis*-enol the bulky substituent points towards the OH group resulting in a steric energetic penalty. The thresholds shown in Figure 6 are for the lowest calculated pathway for each carbonyl. Energies for tautomerisation to all possible enol isomers are reported in Table S2, and tautomerisation geometries are shown in Figure S4.

Keto-enol tautomerisation energies have been previously calculated for acetaldehyde, propanal, butanal, and acetone, with high level theory including CCSD(T)/aug–cc-pVTZ and G3. CCSD(T) is often considered the 'gold standard' in practical quantum chemical calculations, and the composite method G3 is known to be accurate for S_0 carbonyls.[70–72] The B2GP-PLYP/def2-TZVP results calculated in this paper are in good agreement with these previous values, and follow the same energetic ordering (Table S1).

The tautomerisation thresholds for all the linear aldehydes in Figure 6 are in a narrow energy range (278–281 kJ/mol), indicating chain extension has no effect on keto-enol tautomerisation thresholds as long as the bulky alkyl group can be oriented *trans* to the enol OH group. This is not the case for the α-branched 2-methylpropanal, where the enol has a steric penalty from the α-methyl group, leading to the highest keto-enol tautomerisation threshold calculated here (296 kJ/mol).

The tautomerisation thresholds for ketones are also in a narrow range (270–276 kJ/mol), ∼5 kJ/mol lower than the corresponding aldehydes. In the case of asymmetrically substituted ketones, hydrogen transfer from the alternate ketone alkyl substituent is often very close in energy to the *trans*-enol threshold shown in Figure 6, provided the H-transfer from the alternate alkyl substituent also forms a *trans*-enol (Table S2). All linear aldehydes are calculated here to have a keto-enol tautomerisation threshold close to, or below, the threshold calculated for acetaldehyde. According to these calculations and the observation of keto-enol tautomerisation in acetaldehyde, all linear aldehydes and ketones should therefore also have energetically accessible keto-enol tautomerisation pathways.

The α,β-unsaturated carbonyls are calculated to have some of the highest keto-enol tautomerisation thresholds, except in the case of asymmetric ketones where the hydrogen transfer originates from an aliphatic group (*c.f* acrolein and crotonaldehyde to methyl vinyl ketone in Figure 6).

Glycolaldehyde is the only example of a carbonyl with an electron withdrawing functional group in Figure 6, and for this molecule the barrier is predicted to be lowered by 8 kJ/mol compared to acetaldehyde. It would thus appear that electron withdrawing heteroatoms may result in minor decreases in keto–enol tautomerisation thresholds, but it is difficult to draw general conclusions from one example. Regardless,

the barrier for glycolaldehyde is predicted to lie within the energetic range spanned by other carbonyls.

In light of how low the keto–enol tautomerisation barriers are predicted to be, below 300 kJ/mol for all species, it would be expected that this phototautomerisation pathway is energetically accessible in all relevant carbonyls. This has the aforementioned implication that atmospheric reactions following phototautomerisation to the enol can occur in a majority of carbonyl species present in the troposphere. Even if the eventuating QY of organic acid production from each of these species is small, the cumulative effect of enol phototautomerisation in most atmospheric carbonyls could potentially account for a large proportion of the missing organic acid sources in the atmospheric models.

Enal–ketene tautomerisation

There has been recent interest in the formation of ketenes (R′RC=C=O) as atypical and relatively uncharacterised photoproducts of carbonyl photolysis reactions. The 4-centre H_2–loss mechanisms outlined earlier are also able to form ketene compounds. This includes the formation of ketene (ethenone, $H_2C{=}C{=}O$) from the 4-centre H_2–loss TS of acetaldehyde, which has recently been characterised and shown to have unusual product state distributions.[43] Similarly methylketene (prop-1-en-1-one, $CH_3{-}CH{=}C{=}O$) is detected in low QY as a photoproduct of propanal.[50]

However, in enals, there is another potential mechanism to form ketenes that does not involve H_2–loss. This alternative mechanism is demonstrated by the appearance of methylketene as a minor photoproduct following photolysis of acrolein, and dimethylketene following photolysis of methacrolein, across the 285–345 nm wavelength range.[22] Mechanisms and TSs for these enal–ketene tautomerisations are calculated here for acrolein, methacrolein, and crotonaldehyde. Their geometrically labelled TS structures are shown in Figures 7a, 7b, and 7c, respectively.

As can be seen in Figure 7 the structural parameters of the TS geometries for the S_0 enal–ketene tautomerisations in all three enals are

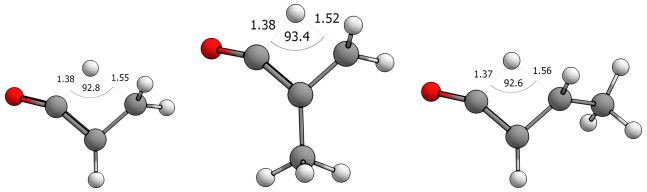

(a) Acrolein **(b)** Methacrolein **(c)** Crotonaldehyde

Figure 7: Transition state structures for the S_0 enal–ketene tautomerisation of acrolein (a), methacrolein (b), and crotonaldehyde (c) computed at the B2GP-PLYP/def2-TZVP level of theory. Bond lengths are shown in Å and angles in degrees.

almost identical. These TSs involve a 1,3-H shift from the formyl-hydrogen to the β-carbon on the main alkyl chain. The distances of the formyl-carbons to the formyl-hydrogens are all 1.37–1.38 Å, which is shorter than the 1.52–1.56 Å distances of formyl-hydrogens to the β-carbons. The ∠formyl-C···H···β-C angles are also similar between the TS geometries, in a 92.6–93.4° range. From these calculations, α-branching or main alkyl chain extension has negligible effect on the configuration of the enal–ketene tautomerisation TSs, and this is reflected in the similar reaction thresholds predicted for the three enals: 297, 291, and 299 kJ/mol for acrolein, methacrolein, and crotonaldehyde, respectively. In the absence of further calculations or experimental data on additional species, a simplistic SAR is that S_0 enal–ketene tautomerisation thresholds for all enal species are approximately 300 kJ/mol, regardless of structure.

Competition between S_0 reactions in carbonyl photolysis experiments

Saturated carbonyls

The calculated energetic thresholds of possible S_0 photolysis reactions in the preceding sections, and SARs derived thereof, can now be applied to interpreting the results of FT-IR experiments. The PhD work of Kharazmi has experimentally observed, following photolysis, significant concerted S_0 reaction QYs in the saturated carbonyls: propanal, 2-methylpropanal, 2-methylbutanal, and pentan-2-one.[50]

In particular, the QYs for the TF reaction lie in the range of 3–5%, except for 2-methylpropanal

where it was 12%. This demonstrates that ground state photolysis reactions are not confined only to molecules that have raised excited state dissociation thresholds (*e.g.* α,β-unsaturated carbonyls), albeit the S_0 TF QYs in saturated species become most significant when the photolysis energy is near or below predicted T_1 NTI thresholds. The highest TF QYs were observed at 330 nm (362.5 kJ/mol) photolysis, which is consistent with the low ($\sim$ 300 kJ/mol) predicted TF thresholds for saturated carbonyls in Table 1.

The high TF QY for 2-methypropanal was argued to be due to an increase in reaction path degeneracy: the α-methyl group in 2-methylpropanal means there are 6 hydrogens in the β-position to undergo TF with the formyl-hydrogen, whereas unbranched species only have 2 or 3 β-hydrogens. The energetic thresholds in Figure 3 support this explanation, the S_0 TF threshold of 2-methylpropanal is predicted to be slightly higher than in the linear aldehydes, and so the observed increase in QY must arise from an increased overall TF rate coefficient which is likely due to reaction path degeneracy.

For saturated carbonyls, the NTIII threshold for each molecule is above the TF threshold but below the decarbonylation threshold. From an energetic perspective this means alkene formation from unimolecular dissociation should be predominately from the TF channel rather than from NTIII reactions in these species. Similarly, the primary formation of CO from decarbonylation should be a minor channel, with a QY lower than both the TF and NTIII pathways. In light of this, the NTIII reaction should be more readily accessible than decarbonylation, so while both perhaps occur with low QYs, the NTIII reaction should be considered in the interpretation of alkene photoproduct QYs. These conclusions are useful when interpreting the sources of photoproducts in a "medium" timescale (minutes) FT-IR photolysis experiment.

α,β-Unsaturated carbonyls

Recent photolysis experiments in the actinic range by Lee on acrolein and methacrolein reveal the importance of the S_0 photolysis reactions in these two α,β-unsaturated species.[22] The IR absorption signal for CO appears, following photolysis, in the FT-IR spectra of both species. The observed CO could arise from: decarbonylation, TF, or secondary radical reactions following NTI dissociation. Since the H_2 photoproduct from TF is IR-inactive, the TF co-products are used for unambiguous identification of TF reaction. These TF photolysis co-products are: ethyne from acrolein; or propyne and allene from methacrolein, originating from *anti* and *syn* conformations, respectively.

Similarly, the QY of decarbonylation can be determined from FT-IR observation of ethene from acrolein and propene from methacrolein. However, several possible channels could generate these photoproducts, including secondary radical reactions in the photolysis chamber. Disambiguation of decarbonylation QYs is therefore difficult and, ideally, requires kinetic modelling. Regardless, the QYs of decarbonylation products in methacrolein (detectable in trace amounts) are significantly lower than those from TF (1–2% for propyne and 0.2–0.5% for allene).[22] This is consistent with the predicted S_0 photolysis thresholds in Table 1, where TF thresholds are $\sim$20–30 kJ/mol lower than decarbonylation thresholds for the enals.

This quantification of S_0 photoproducts of acrolein and methacrolein is ultimately of importance to atmospheric chemistry, as they are VOCs with high atmospheric abundance and may be a currently unquantified source of H_2 in the atmosphere. Methacrolein is particularly important in tropospheric chemistry as an oxidation product of of isoprene.[73–75] Contemporary models underestimate the concentration of H_2 in the atmosphere compared to field observations by $\sim$30–50%, indicative that photolytic sources of H_2 are missing from atmospheric models.[76,77] Photolysis of VOCs in the troposphere is the main source of H_2 in the atmosphere, and is estimated to account for 40–70% of total atmospheric H_2.[78–81] Formaldehyde is known to account for $\sim$50% of this photolytic H_2,[82] while the mechanism(s) generating the other half of photolytic H_2 is unknown.[83] Since both TF and H_2-loss reactions can generate H_2 photolytically on the ground state, and are energetically ac-

cessible across all carbonyl species according to these calculations, the cumulative impact of these ground state H_2 forming channels need to be quantified to assess whether they are a significant omission from atmospheric models.

Besides energetic thresholds, other considerations must be taken into account to predict photolysis rate coefficients. These include: how conformationally 'loose' the transition state is, the corresponding density of states at the TS, and the reaction path degeneracy; all of which factor into which S_0 reactions will dominate. Accordingly, both theoretical kinetics studies[84,85] and master equation modelling[86] are warranted. The quantities calculated in this paper are those required as the basis for theoretical kinetics modelling.

Conclusions

The calculations in this paper demonstrate that a range of potential ground state photochemical pathways cannot be ignored in the tropospheric photochemistry of carbonyls. The energetic thresholds for these S_0 reactions are some of the lowest calculated amongst carbonyl reactions, on all electronic states.[14,87] The TF and keto–enol tautomerisation reactions in particular are predicted to have reaction thresholds of 300 kJ/mol or lower, for most carbonyl species. Even if these S_0 pathways are present in low QYs for individual carbonyl species, the lack of inclusion of ground state photochemistry in the photolysis schemes of most atmospheric models could be leading to deficiencies in predicted concentrations of atmospheric species, particularly when the cumulative effect across all carbonyl species is considered.

Outside the tropospheric context, there have been determinations of an S_1/S_0 conical intersection (CI) at elongated C−C bond lengths, in both acetaldehyde and acetone.[88–90] These S_1/S_0 CIs are accessed at energies above the 400 kJ/mol (300 nm) upper photon energy in the troposphere. In photolysis experiments above 400 kJ/mol, these CIs may be common to other carbonyl species, and lead to increased importance of ground state photochemistry. Indeed, this is consistent with observed increases in QYs of S_0 reactions, such as decarbonylation, in photolysis experiments at energies above 400 kJ/mol in species such as: acetaldehyde,[88] propanal,[91] 2-methylpropanal,[92] butanal,[54] and pentanal.[93]

Because S_0 is accessed following photoexcitation only *via* electronic surface crossing processes, during which collisions and internal energy redistribution can occur, a comprehensive understanding of ground state photochemistry in carbonyls requires accurate rates of: intersystem crossing and internal conversion,[16] collisional energy transfer,[94,95] and intramolecular vibrational energy distribution;[96] all of which are areas of ongoing theoretical study.

Experimental determination of QYs for these S_0 reactions has been hampered since the photoproducts are often either: transient (tautomerisation), IR-inactive (H_2 formation), or ambiguous as they can arise from multiple mechanisms (decarbonylation *vs.* roaming). Since photoexcited carbonyls that cross to S_0 are generated with a large amount of internal energy in comparison to the low S_0 barriers calculated here, S_0 pathways will be less affected by collisional cooling than excited state reactions. Therefore further combination of pressure and wavelength-dependent photolysis studies with theoretical modelling should serve to: disambiguate the mechanistic source of photoproducts, assign the electronic state from which they arise, and allow development of a predictive understanding of how carbonyl species photolyse in the atmosphere based upon their structural features.

Acknowledgement This work was supported by the Australian Research Council (grant DP160101792). It was also supported by grants of computer time under the Merit Allocation Scheme on the NCI National Facility at the Australian National University, as well as computer time on the computational cluster Katana supported by the Faculty of Science, UNSW Australia, and the computational cluster Artemis supported by the Sydney Informatics Hub at the University of Sydney. KNR recognises an Australian Government Research Training Program (RTP) scholarship.

Supporting Information Available: The

Supporting Information contains: labelled S_0 transitions state structures for the decarbonylation, triple fragmentation, Norrish Type III β-hydrogen transfer, and keto-enol tautomerisation reaction mechanisms; comparison between keto-enol tautomerisation energies using different quantum chemical methods; keto-enol tautomerisation energies for all possible enol isomers from each parent carbonyl. (PDF) Cartesian co-ordinates for all optimised transition states. (ZIP) This material is available free of charge via the Internet at http://pubs.acs.org/.

Computational Methods

S_0 calculations were performed with the B2GP-PLYP double-hybrid density functional,[51] using the def2-TZVP canonical basis set[97] and the RIJK resolution of the identity approximation with the def2/JK and def2-TZVP/C auxiliary basis sets. The use of the RIJK approximation, and the 'RI-' prefix, are taken as implicit. All singlepoint energies, geometry optimisations and frequency calculations used this same B2GP-PLYP/def2-TZVP level of theory. All zero-point energies are scaled with the 0.9752 scaling factor derived for this level of theory.[98]

Transition states are confirmed by a single imaginary frequency, whose motion corresponds to the desired reaction coordinate, in the computed Hessian at the TS geometry. Intrinsic reaction coordinate (IRC) calculations were performed to ensure that the imaginary modes connect the desired reactant and product minima. In order to cut down on computational burden, IRC calculations were not performed in certain cases where a TS had a structure and reaction coordinate directly analogous to a homologous molecule where an IRC had already been calculated to verify the reaction mechanism.

References

(1) Townsend, D.; Lahankar, S. A.; Lee, S. K.; Chambreau, S. D.; Suits, A. G.; Zhang, X.; Rheinecker, J.; Harding, L. B.; Bowman, J. M. The roaming atom: Straying from the reaction path in formaldehyde decomposition. *Science* **2004**, *306*, 1158–1161, DOI: 10.1126/science.1104386.

(2) Bowman, J. M.; Houston, P. L. Theories and simulations of roaming. *Chem. Soc. Rev.* **2017**, DOI: 10.1039/C7CS00578D.

(3) Houston, P. L.; Wang, X.; Ghosh, A.; Bowman, J. M.; Quinn, M. S.; Kable, S. H. Formaldehyde roaming dynamics: Comparison of quasi-classical trajectory calculations and experiments. *J. Chem. Phys.* **2017**, *147*, 013936, DOI: 10.1063/1.4982823.

(4) Tsai, P.-Y.; Hung, K. C.; Li, H. K.; Lin, K. C. Photodissociation of propionaldehyde at 248 nm: Roaming pathway as an increasingly important role in large aliphatic aldehydes. *J. Phys. Chem. Lett.* **2014**, *5*, 190–195, DOI: 10.1021/jz402329g.

(5) Tsai, P.-Y.; Li, H.-K.; Kasai, T.; Lin, K.-C. Roaming as the dominant mechanism for molecular products in the photodissociation of large aliphatic aldehydes. *Phys. Chem. Chem. Phys.* **2015**, *17*, 23112–23120, DOI: 10.1039/C5CP03408F.

(6) So, S.; Wille, U.; Da Silva, G. Photoisomerization of Methyl Vinyl Ketone and Methacrolein in the Troposphere: A Theoretical Investigation of Ground-State Reaction Pathways. *ACS Earth Space Chem.* **2018**, *2*, 753–763, DOI: 10.1021/acsearthspacechem.8b00066.

(7) Toulson, B. W.; Fishman, D. A.; Murray, C. Photodissociation dynamics of acetone studied by time-resolved ion imaging and photofragment excitation spectroscopy. *Phys. Chem. Chem. Phys.* **2018**, *20*, 2457–2469, DOI: 10.1039/C7CP07320H.

(8) Andrews, D. U.; Heazlewood, B. R.; Maccarone, A. T.; Conroy, T.; Payne, R. J.; Jordan, M. J. T.; Kable, S. H. Photo-Tautomerization of Acetaldehyde to Vinyl Alcohol: A Potential Route to Tropospheric Acids. *Science* **2012**, *337*, 1203–1206, DOI: 10.1126/science.1220712.

(9) Kurosaki, Y. Photodissociation of Acetaldehyde , $C_3CHO \rightarrow CH_4 + CO$: II. Direct Ab Initio Molecular Dynamics Study.

Chem. Phys. Lett. **2006**, *421*, 549–553, DOI: 10.1016/j.cplett.2006.02.015.

(10) Rickard, A.; Young, J. The Master Chemical Mechanism (MCM) v3.2. http://mcm.leeds.ac.uk/MCM.

(11) Jenkin, M. E.; Saunders, S. M.; Derwent, R. G.; Pilling, M. J. Development of a reduced speciated VOC degradation mechanism for use in ozone models. *Atmos. Environ.* **2002**, *36*, 4725–4734, DOI: 10.1016/S1352-2310(02)00563-0.

(12) Harvard Atmospheric Chemistry Modeling Group, GEOS-Chem 12.4.0. http://acmg.seas.harvard.edu/geos/index.html.

(13) Wild, O.; Zhu, X.; Prather, M. J. Fast-J: Accurate simulation of in- and below-cloud photolysis in tropospheric chemical models. *J. Atmos. Chem.* **2000**, *37*, 245–282, DOI: 10.1023/A:1006415919030.

(14) Rowell, K. N.; Kable, S. H.; Jordan, M. J. T. Structural Effects on the Norrish Type I α-Bond Cleavage of Tropospherically Important Carbonyls. *The Journal of Physical Chemistry A* **2019**, *123*, 10381–10396, DOI: 10.1021/acs.jpca.9b05534, PMID: 31675237.

(15) Godunov, I. A.; Yakovlev, N. N.; Khimii, Z. S. Experimental structural and conformational studies of carbonyl molecules in the ground and lower excited states. *J. Struct. Chem.* **1995**, *36*, 238–253, DOI: 10.1007/BF02578062.

(16) Corrigan, M. E. Modelling the Photochemistry of Acetaldehyde. Honours thesis, The University of Sydney, 2015.

(17) El-Sayed, M. A. Spin-Orbit Coupling and the Radiationless Processes in Nitrogen Heterocyclics. *Chem. Phys.* **1961**, *38*, 2834–2838.

(18) Heicklen, J.; Noyes, W. A. The Photolysis and Fluorescence of Acetone and Acetone-Biacetyl Mixtures. *J. Am. Chem. Soc.* **1959**, *81*, 3858–3863, DOI: 10.1021/ja01524a016.

(19) Copeland, R. A.; Crosley, D. R. Radiative, collisional and dissociative processes in triplet acetone. *Chemical Physics Letters* **1985**, *115*, 362–368, DOI: 10.1016/0009-2614(85)85149-6.

(20) Ritchie, G. *Atmospheric Chemistry: From Surface to Stratosphere*; World Scientific: Oxford, 2017.

(21) Kesselmeier, J.; Staudt, M. Biogenic Volatile Organic Compunds (VOC): An Overview on Emission, Physiology and Ecology. *J. Atmos. Chem.* **1999**, *33*, 23–88, DOI: 10.1023/A:1006127516791.

(22) Lee, A. D. C. F. An Investigation of the Production of H_2 from the Photolysis of Plant Based Aldehydes. Honours thesis, The University of New South Wales, 2018.

(23) Lary, D. J.; Shallcross, D. E. Central role of carbonyl compounds in atmospheric chemistry. *J. Geophys. Res. Atmos.* **2000**, *105*, 19771–19778, DOI: 10.1029/1999JD901184.

(24) Atkinson, R.; Arey, J. Atmospheric Degradation of Volatile Organic Compounds. *Chem. Rev.* **2003**, *103*, 4605–4638, DOI: 10.1021/cr0206420.

(25) Tanner, R. L.; Zielinska, B.; Uberna, E.; Harshfield, G.; McNichol, A. P. Concentrations of carbonyl compounds and the carbon isotopy of formaldehyde at a coastal site in Nova Scotia during the NARE summer intensive. *J. Geophys. Res. Atmos.* **1996**, *101*, 28961–28970, DOI: 10.1029/95jd03574.

(26) Warneck, P.; Moortgat, G. K. Quantum yields and photodissociation coefficients of acetaldehyde in the troposphere. *Atmos. Environ.* **2012**, *62*, 153–163, DOI: 10.1016/j.atmosenv.2012.08.024.

(27) Zhu, L.; Tang, Y.; Chen, Y.; Cronin, T. Wavelength-dependent photolysis of C3-C7 aldehydes in the 280-330 nm region. *Spectrosc. Lett.* **2009**, *42*, 467–478, DOI: 10.1080/00387010903267195.

(28) Heazlewood, B. R.; Rowling, S. J.; Maccarone, A. T.; Jordan, M. J.; Kable, S. H. Photochemical formation of HCO and CH_3 on the ground S_0 ($^1A'$) state of CH_3CHO. *J. Chem. Phys.* **2009**, *130*, 054310, DOI: 10.1063/1.3070517.

(29) de Wit, G.; Heazlewood, B. R.; Quinn, M. S.; Maccarone, A. T.; Nauta, K.; Reid, S. A.; Jordan, M. J. T.; Kable, S. H. Product state

and speed distributions in photochemical triple fragmentations. *Faraday Discuss.* **2012**, *157*, 227, DOI: 10.1039/c2fd20015e.

(30) Morajkar, P.; Bossolasco, A.; Schoemaecker, C.; Fittschen, C. Photolysis of CH3CHO at 248 nm: Evidence of triple fragmentation from primary quantum yield of CH3 and HCO radicals and H atoms. *J. Chem. Phys.* **2014**, *140*, 214308, DOI: 10.1063/1.4878668.

(31) Tang, Y.; Zhu, L.; Chu, L. T.; Xiang, B. Cavity ring-down spectroscopic study of acetaldehyde photolysis in the gas phase, on aluminum surfaces, and on ice films. *Chem. Phys.* **2006**, *330*, 155–165, DOI: 10.1016/j.chemphys.2006.08.005.

(32) Moortgat, G. K.; Meyrahn, H.; Warneck, P. Photolysis of acetaldehyde in air: CH4, CO and CO2 quantum yields. *ChemPhysChem* **2010**, *11*, 3896–3908, DOI: 10.1002/cphc.201000757.

(33) Bowman, J. M.; Shepler, B. C. Roaming Radicals. *Annu. Rev. Phys. Chem.* **2011**, *62*, 531–553, DOI: 10.1146/annurev-physchem-032210-103518.

(34) Heazlewood, B. R.; Jordan, M. J. T.; Kable, S. H.; Selby, T. M.; Osborn, D. L.; Shepler, B. C.; Braams, B. J.; Bowman, J. M. Roaming is the dominant mechanism for molecular products in acetaldehyde photodissociation. *Proc. Natl. Acad. Sci. U.S.A.* **2008**, *105*, 12719–12724, DOI: 10.1073/pnas.0802769105.

(35) Andrews, D. U.; Kable, S. H.; Jordan, M. J. A phase space theory for roaming reactions. *J. Phys. Chem. A* **2013**, *117*, 7631–7642, DOI: 10.1021/jp405582z.

(36) Mauguière, F. A.; Collins, P.; Kramer, Z. C.; Carpenter, B. K.; Ezra, G. S.; Farantos, S. C.; Wiggins, S. Roaming: A Phase Space Perspective. *Annu. Rev. Phys. Chem.* **2017**, *68*, 499–524, DOI: 10.1146/annurev-physchem-052516-050613.

(37) Rubio-Lago, L.; Amaral, G. A.; Arregui, A.; González-Vázquez, J.; Bañares, L. Imaging the molecular channel in acetaldehyde photodissociation: Roaming and transition state mechanisms. *Phys. Chem. Chem. Phys.* **2012**, *14*, 6067–6078, DOI: 10.1039/c2cp22231k.

(38) Houston, P. L.; Conte, R.; Bowman, J. M. Roaming under the Microscope: Trajectory Study of Formaldehyde Dissociation. *J. Phys. Chem. A* **2016**, *120*, 5103–5114, DOI: 10.1021/acs.jpca.6b00488.

(39) Mauguière, F. A. L.; Collins, P.; Kramer, Z. C.; Carpenter, B. K.; Ezra, G. S.; Farantos, S. C.; Wiggins, S. Phase Space Structures Explain Hydrogen Atom Roaming in Formaldehyde Decomposition. *J. Phys. Chem. Lett.* **2015**, *6*, 4123–4128, DOI: 10.1021/acs.jpclett.5b01930.

(40) Clubb, A. E.; Jordan, M. J. T.; Kable, S. H.; Osborn, D. L. Phototautomerization of Acetaldehyde to Vinyl Alcohol: A Primary Process in UV-Irradiated Acetaldehyde from 295 to 335 nm. *The Journal of Physical Chemistry Letters* **2012**, *3*, 3522–3526, DOI: 10.1021/jz301701x, PMID: 26290982.

(41) Shaw, M. F.; Sztáray, B.; Whalley, L. K.; Heard, D. E.; Millet, D. B.; Jordan, M. J.; Osborn, D. L.; Kable, S. H. Phototautomerization of acetaldehyde as a photochemical source of formic acid in the troposphere. *Nature Comm.* **2018**, *9*, 1–7, DOI: 10.1038/s41467-018-04824-2.

(42) Heazlewood, B. R.; Maccarone, A. T.; Andrews, D. U.; Osborn, D. L.; Harding, L. B.; Klippenstein, S. J.; Jordan, M. J. T.; Kable, S. H. Near-threshold H/D exchange in CD3CHO photodissociation. *Nature Chemistry* **2011**, *3*, 443–448, DOI: 10.1038/nchem.1052.

(43) Harrison, A. W.; Kharazmi, A.; Shaw, M. F.; Quinn, M. S.; Lee, K. L. K.; Nauta, K.; Rowell, K. N.; Jordan, M. J. T.; Kable, S. H. Dynamics and Quantum Yields of H_2 + CH_2CO as a Primary Photolysis Channel in CH_3CHO. *Phys. Chem. Chem. Phys.* **2019**, 14284–14295, DOI: 10.1039/c8cp06412a.

(44) Atkinson, R.; Baulch, D. L.; Cox, R. A.; Crowley, J. N.; Hampson, R. F.; Hynes, R. G.; Jenkin, M. E.; Rossi, M. J.; Troe, J. IUPAC Task Group on Atmospheric Chemical Kinetic Data Evaluation – Data Sheet P2. *Atmos. Chem. Phys.* **2004**, *4*, 1461–1738, DOI: 10.5194/acp-4-1461-2004.

(45) Wallington, T. J.; Ammann, M.; Cox, R. A.; Crowley, J. N.; Herrmann, H.; Jenkin, M. E.; McNeill, V.; Mellouki, A.; Troe, J. IUPAC Task Group on Atmospheric Chemical Kinetic Data Evaluation. http://iupac.pole-ether.fr/.

(46) Eastham, S. D.; Weisenstein, D. K.; Barrett, S. R. Development and evaluation of the unified tropospheric–stratospheric chemistry extension (UCX) for the global chemistry-transport model GEOS-Chem. *Atmospheric Environment* **2014**, *89*, 52–63, DOI: 10.1016/j.atmosenv.2014.02.001.

(47) Atkinson, R.; Baulch, D.; Cox, Evaluated kinetic and photochemical data for atmospheric chemistry: Volume II – gas phase reactions of organic species. *Atmos. Chem. Phys.* **2006**, *6*, 3625–4055, DOI: https://doi.org/10.5194/acp-6-3625-2006.

(48) Jenkin, M. E.; Saunders, S. M.; Pilling, M. J. The tropospheric degradation of volatile organic compounds: A protocol for mechanism development. *Atmos. Environ.* **1997**, *31*, 81–104, DOI: 10.1016/S1352-2310(96)00105-7.

(49) Shaw, M. F. Photochemical Formation of Enols from Carbonyls. Ph.D. thesis, The University of Sydney, 2017.

(50) Kharazmi, A. Investigating the Complex Photochemistry of Atmospheric Carbonyls. Ph.D. thesis, The University of New South Wales, 2019.

(51) Karton, A.; Tarnopolsky, A.; Lamère, J.-F.; Schatz, G. C.; Martin, J. M. L. Highly Accurate First-Principles Benchmark Data Sets for the Parametrization and Validation of Density Functional and Other Approximate Methods. Derivation of Robust, Generally Applicable, Double-Hybrid Functional for Thermochemistry and Thermochemical Kinetics. *J. Phys. Chem. A* **2008**, *112*, 12868, DOI: 10.1021/jp801805p.

(52) Keller-Rudek, G. K., Hannelore Moortgat; Sander, R.; Sörensen, R. The MPI-Mainz UV/VIS Spectral Atlas of Gaseous Molecules of Atmospheric Interest. 2019; www.uv-vis-spectral-atlas-mainz.org.

(53) Gorin, E. Photolysis of Aldehydes and Ketones in the Presence of Iodine Vapor. *The J. Chem. Phys.* **1939**, *7*, 256–264, DOI: 10.1063/1.1750427.

(54) Blacet, F. E.; Calvert, J. G. The Photolysis of Aliphatic Aldehydes. XV. The Butyraldehydes with Iodine Vapor. *J. Am. Chem. Soc.* **1951**, *73*, 667–674, DOI: 10.1021/ja01146a049.

(55) Morioka, T.; Nishizawa, A.; Furukawa, T.; Tobisu, M.; Chatani, N. Nickel-mediated decarbonylation of simple unstrained ketones through the cleavage of carbon-carbon bonds. *J. Am. Chem. Soc.* **2017**, *139*, 1416–1419, DOI: 10.1021/jacs.6b12293.

(56) Leighton, P. A.; Levanas, L. D.; Blacet, F. E.; Rowe, R. D. The Photolysis of the Aliphatic Aldehydes. IV. n- and Isobutyraldehydes. *J. Am. Chem. Soc.* **1937**, *59*, 1843–1849, DOI: 10.1021/ja01289a019.

(57) Pople, J. A. Quantum Chemical Models (Nobel Lecture). *Angewandte Chemie International Edition* **1999**, *38*, 1894–1902, DOI: 10.1002/(SICI)1521-3773(19990712)38:13/14<1894::AID-ANIE1894>3.0.CO;2-H.

(58) Blacet, B. F. E.; Heldman, J. D.; Heldman, J. D. The Photolysis of the Aliphatic Aldehydes . Acetaldehyde and Iodine Mixtures. *J. Am. Chem. Soc.* **1942**, *64*, 889–893, DOI: 10.1021/ja01256a044.

(59) Moortgat, G. K.; Seiler, W.; Warneck, P. Photodissociation of HCHO in air: CO and H2 quantum yields at 220 and 300 K. *J. Chem. Phys.* **1983**, *78*, 1185–1190, DOI: 10.1063/1.444911.

(60) Tadić, J.; Moortgat, G. K.; Wirtz, K. Photolysis of glyoxal in air. *J. Photochem. and Photobiology A: Chemistry* **2006**, *177*, 116–124, DOI: 10.1016/j.jphotochem.2005.10.010.

(61) Chen, Y.; Wang, W.; Zhu, L. Wavelength-dependent photolysis of methylglyoxal in the 290-440 nm region. *J. Phys. Chem. A* **2000**, *104*, 11126–11131, DOI: 10.1021/jp002262t.

(62) Zhu, L.; Kellis, D.; Ding, C.-F. Photolysis of glyoxal at 193, 248, 308 and 351 nm. *Chem. Phys. Lett.* **1996**, *257*,

487–491, DOI: https://doi.org/10.1016/0009-2614(96)00570-2.

(63) Bacher, C.; Tyndall, G. S.; Orlando, J. J. The atmospheric chemistry of glycolaldehyde. *J. Atmos. Chem.* **2001**, *39*, 171–189, DOI: 10.1023/A:1010689706869.

(64) Zhu, C.; Zhu, L. Photolysis of glycolaldehyde in the 280–340 nm region. *J. Phys. Chem. A* **2010**, *114*, 8384–8390, DOI: 10.1021/jp104497d.

(65) So, S.; Wille, U.; Da Silva, G. A Theoretical Study of the Photoisomerization of Glycolaldehyde and Subsequent OH Radical-Initiated Oxidation of 1,2-Ethenediol. *J. Phys. Chem. A* **2015**, *119*, 9812–9820, DOI: 10.1021/acs.jpca.5b06854.

(66) Cui, G.; Fang, W. Mechanistic photodissociation of glycolaldehyde: Insights from ab initio and RRKM calculations. *ChemPhysChem* **2011**, *12*, 1351–1357, DOI: 10.1002/cphc.201000968.

(67) Zahra, A.; Noyes, W. A. The photochemistry of methyl isopropyl ketone. *J. Phys. Chem.* **1965**, *69*, 943–948, DOI: 10.1021/j100887a041.

(68) Keeffe, J. R.; Kresge, A. J.; Schepp, N. P. Generation of Simple Enols by Photooxidation. Keto-Enol Equilibrium Constants of Some Aliphatic Systems in Aqueous Solution. *J. Am. Chem. Soc.* **1988**, *110*, 1993–1995, DOI: 10.1021/ja00214a069.

(69) Heazlewood, B. R. Unusual Photodissociation Dynamics in Acetaldehyde and Deuterated Acetaldehyde. Ph.D. thesis, The University of Sydney, 2011.

(70) Curtiss, L. A.; Raghavachari, K.; Redfern, P. C.; Rassolov, V.; Pople, J. A. Gaussian-3 (G3) theory for molecules containing first and second-row atoms. *J. Chem. Phys.* **1998**, *109*, 7764–7776, DOI: 10.1063/1.477422.

(71) Balabin, R. M. The keto-enol equilibrium in substituted acetaldehydes: focal-point analysis and ab initio limit. *Mol. Phys.* **2011**, *109*, 2341–2351, DOI: 10.1080/00268976.2011.587457.

(72) Simmie, J. M.; Somers, K. P. Benchmarking Compound Methods (CBS-QB3, CBS-APNO, G3, G4, W1BD) against the Active Thermochemical Tables: A Litmus Test for Cost-Effective Molecular Formation Enthalpies. *The J. Phys. Chem. A* **2015**, *119*, 7235–7246, DOI: 10.1021/jp511403a.

(73) Bonn, B.; Magh, R.-K.; Rombach, J.; Kreuzwieser, J. Biogenic isoprenoid emissions under drought stress: Different responses for isoprene and terpenes. *Biogeosciences Discuss.* **2019**, 1–30, DOI: 10.5194/bg-2019-227.

(74) Wennberg, P. O.; Bates, K. H.; Crounse, J. D.; Dodson, L. G.; McVay, R. C.; Mertens, L. A.; Nguyen, T. B.; Praske, E.; Schwantes, R. H.; Smarte, M. D. et al. Gas-Phase Reactions of Isoprene and Its Major Oxidation Products. *Chem. Rev.* **2018**, 3337–3390, DOI: 10.1021/acs.chemrev.7b00439.

(75) Jenkin, M. E.; Young, J. C.; Rickard, A. R. The MCM v3.3.1 degradation scheme for isoprene. *Atmos. Chem. Phys.* **2015**, *15*, 11433–11459, DOI: 10.5194/acp-15-11433-2015.

(76) Punshon, S.; Moore, R. M. Photochemical production of molecular hydrogen in lake water and coastal seawater. *Mar. Chem.* **2008**, *108*, 215–220, DOI: 10.1016/j.marchem.2007.11.010.

(77) Walter, S.; Kock, A.; Rockmann, T. High-resolution measurements of atmospheric molecular hydrogen and its isotopic composition at thewest african coast of mauritania. *Biogeosciences* **2013**, *10*, 3391–3403, DOI: 10.5194/bg-10-3391-2013.

(78) Ehhalt, D. H.; Rohrer, F. The tropospheric cycle of H_2: a critical review. *Tellus B Chem. Phys. Meteorol.* **2009**, *61B*, 500–535, DOI: 10.1111/j.1600-0889.2009.00416.x.

(79) Rhee, T. S.; Brenninkmeijer, C. A.; Röckmann, T. The overwhelming role of soils in the global atmospheric hydrogen cycle. *Atmos. Chem. Phys.* **2006**, *6*, 1611–1625, DOI: 10.5194/acp-6-1611-2006.

(80) Novelli, P. C. Molecular hydrogen in the troposphere: Global distribution and budget. *J. Geophys. Res. Atmos.* **1999**, *104*, 30427–30444, DOI: 10.1029/1999JD900788.

(81) Price, H.; Jaeglé, L.; Rice, A.; Quay, P.; Novelli, P. C.; Gammon, R. Global budget of molecular hydrogen and its deuterium content: Constraints from ground station, cruise, and aircraft observations. *J. Geophys. Res. Atmos.* **2007**, *112*, D22108, DOI: 10.1029/2006JD008152.

(82) Hauglustaine, D. A. A three-dimensional model of molecular hydrogen in the troposphere. *J. Geophys. Res. Atmos.* **2002**, *107*, 4330, DOI: 10.1029/2001JD001156.

(83) Grant, A.; Witham, C. S.; Simmonds, P. G.; Manning, A. J.; O'Doherty, S. A 15 year record of high-frequency, in situ measurements of hydrogen at Mace Head, Ireland. *Atmos. Chem. Phys.* **2010**, *10*, 1203–1214, DOI: 10.5194/acp-10-1203-2010.

(84) Forst, W. *Theory of Unimolecular Reaction*; Academic Press: London, 1973.

(85) Van Zee, R. D.; Foltz, M. F.; Moore, C. B. Evidence for a second molecular channel in the fragmentation of formaldehyde. *J Chem. Phys.* **1993**, *99*, 1664–1673, DOI: 10.1063/1.465335.

(86) Miller, J. A.; Klippenstein, S. J. Master equation methods in gas phase chemical kinetics. *J. Phys. Chem. A* **2006**, *110*, 10528–10544, DOI: 10.1021/jp062693x.

(87) Rowell, K.; Kable, S.; Jordan, M. J. T. Structural Causes of Singlet/triplet Preferences of Norrish Type II Reactions in Carbonyls. **2020**, DOI: 10.26434/chemrxiv.12941702.v1.

(88) Toulson, B. W.; Kapnas, K. M.; Fishman, D. A.; Murray, C. Competing pathways in the near-UV photochemistry of acetaldehyde. *Phys. Chem. Chem. Phys.* **2017**, *19*, 14276–14288, DOI: 10.1039/c7cp02573d.

(89) Chen, S. L.; Fang, W. H. Insights into photodissociation dynamics of acetaldehyde from ab initio calculations and molecular dynamics simulations. *J. Chem. Phys.* **2009**, *131*, 054306, DOI: 10.1021/jp073875+.

(90) Diau, E. W.-G.; Kötting, C.; Zewail, A. H. Femtochemistry of Norrish Type-I Reactions: I. Experimental and Theoretical Studies of Acetone and Related Ketones on the S_1 Surface. *ChemPhysChem* **2001**, *2*, 273–293, DOI: 10.1002/1439-7641(20010518)2:5<273::AID-CPHC273>3.0.CO;2-H.

(91) Shepson, P. B.; Heicklen, J. The Wavelength and Pressure Dependence of the Photolysis of Proprionaldehyde in Air. *J. Photochem.* **1982**, *19*, 215–227, DOI: 10.1016/0047-2670(82)80024-5.

(92) Chen, Y.; Zhu, L.; Francisco, J. S. Wavelength-Dependent Photolysis of n-Butyraldehyde and i-Butyraldehyde in the 280–330 nm Region. *J. Phys. Chem. A* **2002**, 7755–7763, DOI: 10.1021/JP014544E.

(93) Cronin, T. J.; Zhu, L. Dye Laser Photolysis of n-Pentanal from 280 to 330 nm. *The J. Phys. Chem. A* **1998**, *102*, 10274–10279, DOI: 10.1021/jp982487s.

(94) Jasper, A. W.; Miller, J. A. Lennard-Jones parameters for combustion and chemical kinetics modeling from full-dimensional intermolecular potentials. *Combust. Flame* **2014**, *161*, 101–110, DOI: 10.1016/j.combustflame.2013.08.004.

(95) Jasper, A. W.; Pelzer, K. M.; Miller, J. A.; Kamarchik, E.; Harding, L. B.; Klippenstein, S. J. Predictive a priori pressure-dependent kinetics. *Science* **2014**, *346*, 1212–1215, DOI: 10.1126/science.1260856.

(96) Beil, A.; Luckhaus, D.; Quack, M.; Stohner, J. Intramolecular vibrational redistribution and unimolecular reaction: Concepts and new results on the femtosecond dynamics and statistics in CHBrClF. *Ber. Bunsenges. Phys. Chem.* **1997**, *101*, 311–328, DOI: 10.1002/bbpc.19971010303.

(97) Weigend, F.; Ahlrichs, R. Balanced basis sets of split valence, triple zeta valence and quadruple zeta valence quality for H to Rn: Design and assessment of accuracy. *Phys. Chem. Chem. Phys.* **2005**, *7*, 3297–305, DOI: 10.1039/b508541a.

(98) Kesharwani, M. K.; Brauer, B.; Martin, J. M. Frequency and zero-point vibrational energy scale factors for double-hybrid density functionals (and other selected methods): Can anharmonic force fields be avoided? *J. Phys. Chem. A* **2015**, *119*, 1701–1714, DOI: 10.1021/jp508422u.